Atoms in Molecules Computational Study on the Molecular Structure of $(Cu_2S)_n$ Clusters

Boris Ni and James R. Kramer

School of Geography and Geology, McMaster University, Hamilton, Ontario, Canada

Nick H. Werstiuk*

Department of Chemistry, McMaster University, Hamilton, Ontario, Canada

Received: November 29, 2002

The relative stabilities and molecular structures of $(Cu_2S)_n$ clusters were investigated at the Becke3PW91/6-311+G(d) level and with AIM. Three new $(Cu_2S)_n$ clusters are revealed. Although all Cu−S covalent bonds are confirmed, we find that Cu−Cu covalent bonding implied/assigned in graphical geometrical structures simply on the basis of internuclear distance or overlap populations is not realized in most cases. The asymptotic behavior of stabilization energy with increasing cluster size is explained on the basis of unit coordination.

Introduction

Metal-sulfide molecular clusters play an extremely important role in inorganic and organic chemical processes. For example, iron−sulfur, zinc−sulfur, and copper−sulfur clusters are found in many proteins and serve as catalytic centers in biologically important reactions of ligand exchange, charge transfer, and oxidative degradation.[1−5] In addition, compounds containing ZnS, CdS, and CuS clusters have found novel uses in a variety of industrial applications such as optical and optoelectronic devices, photocatalysts and semiconductors.[5−8] New methods of growing Cu_2S nanowires show promise in generating new materials.[9,10] A number of synthetic metal sulfides containing Cu, Ag, and Hg, exhibit remarkable stability and do not degrade in oxic acidic (pH 0−1) solutions[11] and synthetic Zn−S clusters have been shown to stoichiometrically suppress the acute toxicity of Ag(I) to the water flea, *Daphnia magna*.[12]

Despite the importance of these species, especially in the chemistry of natural organic matter, a detailed theoretical understanding of the molecular structure, the bonding, of the sulfide cluster complexes, the mechanisms of their reactions, and factors that control their stability is lacking. Computational studies are particularly challenging in this field, even for relatively small clusters. Difficulties are encountered in accurate computational studies for a number of reasons; large numbers of electrons are involved and the proper treatment of spin state coupling presents a challenging task.[13,14] Relatively small $(Cu_2S)_n$ clusters with $n < 6$ have not been prepared to this point, so a direct comparison of computational and experimental results is not possible for these species. Even so, the experimental and computational studies of a number of $(Cu_2S)_n$ clusters together with their phosphane-ligated complexes have been reported recently.[15−17] Geometries and relative energies of clusters up to $Cu_{20}S_{10}$ have been studied at the ab initio level using effective core potentials (ECPs). However, a full systematic study of the molecular structure, the bonding, has not been carried out. Currently bonding between atoms, the coordination, in structures derived from graphical programs is assigned on the basis of the average ranges of interatomic distances (or covalent radii of atoms) and not on a rigorous theoretical basis such as provided by atoms in molecules (AIM).[18] Thus, the purpose of our work was to study Cu_2S (**1**) and the clusters Cu_4S_2 (**2**, **3**, **4**, and **5**), Cu_6S_3 (**6**, **7**, and **8**), Cu_8S_4 (**9**, **10**, and **11**), $Cu_{10}S_5$ (**12**), $Cu_{12}S_6$ (**13**), $Cu_{16}S_8$ (**14** and **15**), and $Cu_{20}S_{10}$ (**16**) at a higher level while including all electrons and to investigate the bonding with AIM. We report our results in this publication and compare our findings with those obtained using the ECP method.

Computational Methods

Equilibrium optimized geometries of **1**−**16** were obtained at the DFT Becke3PW91/6-311+G(d) level that includes the Becke−Perdew−Wang (B3PW91) exchange-correlation potential[19] as implemented in Gaussian 98.[20] Unlike previous investigations that involved the MP2 method with effective core potentials (ECPs), we carried out all-electron DFT calculations in order to obtain wave functions necessary for AIM analyses. We chose a DFT method and the 6-311+G(d) basis set because (a) the low computational cost would allow us to study large clusters and (b) several studies[21−23] established that it is important to include polarization and diffuse functions especially in post Hartee-Fock electron−correlation calculations because small basis sets produce significant errors. As a check, we also studied Cu_2S at the MP2(FC)/6-31G(d), MP2(Full)/6-31G(d), MP2(FC)/6-311+G(d) and MP2(Full)/6-311+G(d) levels. Except for Cu_2S, optimizations were performed in stages on the clusters. Initial geometries were obtained with the MM+ force field of HyperChem,[24] with the molecular symmetries being set at this stage. In the next step, optimizations were carried out at the Becke3PW91/3-21G level with the SCF convergence criterion set to 10^{-5} and a virtual orbital shift of 1 au applied. In most cases, it was necessary to increase the SCF iteration limit to 400. After an optimized geometry was obtained with the small basis set, a refined geometry was obtained at the 6-311+G(d) level with the SCF convergence criterion set to 10^{-6}. Single-point calculations with SCF=TIGHT were used to obtain wave functions that were analyzed with the AIMPAC suite of programs[25] and AIM2000.[26] Molecular graphs for **1**−**16** obtained were with AIM2000 and are presented in Figure 1−6. Where possible, we took advantage of the molecular symmetry to decrease computational time. However, in the case of **7**, **8**,

* To whom correspondence should be addressed. E-mail: werstiuk@mcmaster.ca.

10.1021/jp027587j CCC: $25.00
Published on Web 03/29/2003

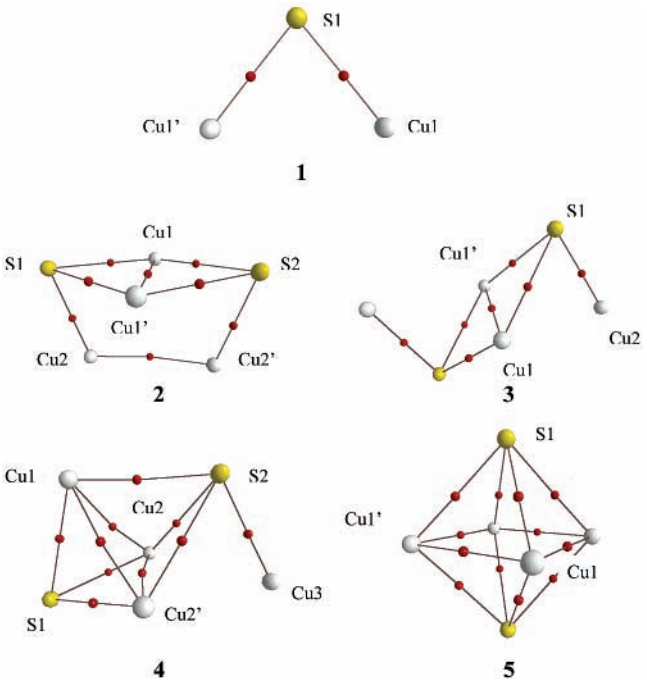

Figure 1. Displays of the molecular graphs of **1** (Cu_2S), **2**, **3**, **4**, and **5** (Cu_4S_2 isomers); copper atoms shown as gray spheres, sulfur atoms as yellow spheres, and bond critical points as red spheres.

9, **11**, and **13**, calculations on the highest symmetry structures failed, and the symmetry had to be reduced to achieve a result. In these cases, structures very close to those expected for the high-symmetry species were obtained with the differences in interatomic distances being less than 0.001 Å.

Results and Discussion

To check the effect of varying the computational method and the size of the basis on geometry and the molecular structure, we studied Cu_2S at the Becke3PW91/6-311+G(d), MP2(FC)/6-31G(d), MP2(Full)/6-31G(d), MP2(FC)/6-311+G(d), and MP2(Full)/6-311+G(d) levels. At the Becke3PW91/6-311+G(d) level, there is no bond path between the copper atoms (Figure 1). In going from Becke3PW91/6-311+G(d) to the MP2(FC)/6-31G(d) level, the Cu−S and Cu1−Cu1′ internuclear distances decreased from 2.114 to 1.995 Å and 2.634 to 2.208 Å, respectively; at the MP2(Full)/6-31G(d) level, there are further very small decreases to 1.994 Å and 2.118 Å. An AIM analysis revealed a bond path between Cu1 and Cu1′ at both MP2/6-31G(d) levels. However, the tenuous nature of the bond was indicated by the low value of $\rho(\mathbf{r}_c)$ (0.36eÅ^{-3}) at the BCP and the proximity of the ring critical point (RCP) to the BCP at the MP2(FC)/6-31G(d) level. In such a case, a small increase in internuclear distance or decrease in the density between the copper atoms would result in the annihilation of the RCP and BCPs. This was realized when MP2(FC)/6-311+G(d) and MP2(Full)/6-311+G(d) calculations were carried out; the Cu1−Cu1′ distances increased by 0.424 Å (to 2.632 Å) and 0.493 Å (to 2.611 Å), respectively. These values are close to the distance (2.634 Å) found at the Becke3PW91/6-311+G(d) level. Of significance is the fact that the copper atoms were no longer connected via a bond path at these higher MP2 levels. In our view, this finding validates the results of all our Becke3PW91/6-311+G(d) calculations. We have also completed an AIM study of the molecular structure of a group of $Cu_xS_y^{-1}$ clusters, prepared and studied in the gas phase by Dance and coworkers,[27,28] at the Becke3PW91/6-311+G(d) and MP2/6-311+G(d) levels. In keeping with our calculations on Cu_2S, identical results were obtained at these levels of theory. We would like to emphasize that the difference in Cu−Cu internuclear distance is not the only factor determining the presence or absence of a covalent bond. AIM analysis of the wave functions obtained with single-point calculations at the Becke3PW91/6-311+G(d)//MP2(FC)/6-31G(d) (Cu−Cu distance 2.208 Å) and MP2(FC)/6-31G(d)//Becke3PW91/6-311+G(d) (Cu−Cu distance 2.634 Å) levels yielded no bond path between the coppers atoms.

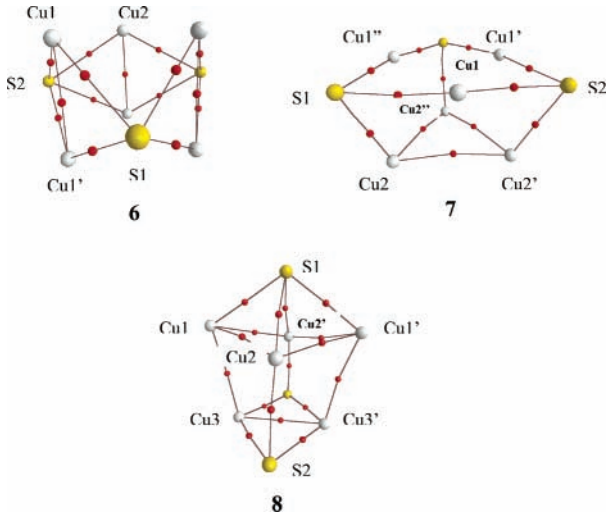

Figure 2. Displays of the molecular graphs of **6**, **7**, and **8** that are Cu_6S_3 isomers; copper atoms shown as gray spheres, sulfur atoms as yellow spheres, and bond critical points as red spheres.

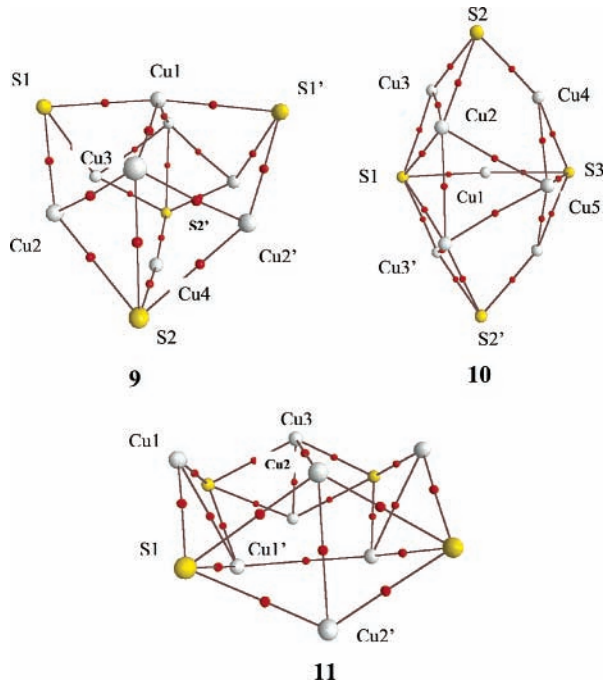

Figure 3. Displays of the molecular graphs of **9**, **10**, and **11** that are Cu_8S_4 isomers; copper atoms shown as gray spheres, sulfur atoms as yellow spheres, and bond critical points as red spheres.

We have found three new $(Cu_2S)_n$ structures, one of which is **9** that turns out to be the most stable isomer of composition Cu_8S_4 (Figure 3). Two other structures are isomers of the composition $Cu_{16}S_8$. Isomers of $Cu_{16}S_8$ were searched to confirm the asymptotic behavior of stabilization energy as discussed below. Selected interatomic distances of **1**−**16** are collected in Table 1 together with the values obtained with ECP calcula-

TABLE 1: Selected Inter-nuclear Distances of $(Cu_2S)n$ Clusters

	S1−Cu1	S1−Cu2	S1−Cu3	S2−Cu2	Cu1−Cu1′	Cu1−Cu2	Cu1−Cu3	Cu2−Cu3	Cu2−Cu2′	Cu3−Cu3′
1	2.114				2.634					
	(2.087)[a]				(2.516)					
2	2.311	2.142			2.376	2.693			2.734	
	(2.264)	(2.118)			(2.185)	(2.608)			(2.729)	
3	2.310	2.134			2.367	2.704				
	(2.263)	(2.114)			(2.172)	(2.651)				
4	2.265	2.280		2.439		2.434		2.559	2.466	
	(2.236)	(2.239)		(2.366)		(2.323)		(2.528)	(2.294)	
5	2.411				2.348					
	(2.363)				(2.213)					
6	2.350				2.353	2.566				
	(2.305)				(2.177)	(2.485)				
7	2.228	2.194			2.728	2.570			2.743	
	(2.186)	(2.176)			(2.655)	(2.483)			(2.652)	
8	2.321	2.292		2.160		2.429	2.600	2.822	2.948	2.358
	(2.314)	(2.234)				2.334	2.492	(2.701)	(2.789)	(2.197)
9	2.309	2.271	2.393	2.216				2.378		
10	2.265	2.409	2.418	2.261		2.806	2.634	2.389	2.564	
	(2.217)	(2.333)	(2.432)	(2.203)		(2.725)	(2.570)	(2.223)	(2.507)	
11	2.286	2.370			2.374	2.650		2.753		
	(2.234)	(2.340)			(2.206)	(2.604)		(2.648)		
12	2.634	2.244	2.480	2.212		2.507	2.290	2.823	2.691	
	(2.619)	(2.190)	(2.416)	(2.174)		(2.426)	(2.142)	(2.687)	(2.628)	
13	2.277				2.566	2.563				
	(2.234)				(2.493)	(2.493)				
14	2.160		2.271	2.336		2.783		2.441	2.583	2.417
15	2.282				2.461	2.670				
16	2.250	2.254	2.214	2.275		2.628	2.736		2.532	3.871
	(2.213)	(2.197)	(2.156)	(2.234)		(2.585)	(2.644)		(2.459)	(3.918)

[a] The values in parentheses correspond to the internuclear distances obtained with effective core potential calculations reported in references 15-17.

TABLE 2: Symmetries, Energies, and Numbers of Cu−S and Cu−Cu Bonds of $(Cu_2S)_n$ Clusters

n	compound	symm	E_T (a.u.)	E_{rel} (kJ/mol)[a]	E_n	*N*(Cu−S)	*N*(Cu−Cu)[a]
1	**1**	C_{2v}	−3679.132972		0.0	2	0(1)
2	**2**	C_{2v}	−7358.352425	0.0	113.5	6	2(6)
	3	C_{2h}	−7358.352399	0.1 (7.1)	113.5	6	1(5)
	4	C_s	−7358.348729	9.7 (22.8)	108.7	7	3(5)
	5	D_{4h}	−7358.334735	46.4 (51.8)	90.3	8	4(4)
3	**6**	D_{3h}	−11037.621394	0.0	194.7	12	3(9)
	7	$\sim C_{3v}$	−11037.617169	11.1 (11.0)	191.0	9	3(9)
	8	$\sim C_{2v}$	−11037.613364	21.1 (17.1)	187.7	10	7(12)
4	**9**	$\sim C_{2v}$	−14716.915342	0.0	251.7	14	6
	10	C_s	−14716.884899	79.9 (0.0)	231.7	14	7(15)
	11	$\sim D_{2d}$	−14716.858601	149.0(72.0)	214.4	16	6(14)
5	**12**	D_{3h}	−18396.200952		281.5	18	9(21)
6	**13**	$\sim O_h$	−22075.546580		327.6	24	0(24)
8	**14**	C_{2h}	−29433.922390	0.0	282.0	28	12
	15	D_{8h}	−29433.581358	896.1	169.9	32	0
10	**16**	D_{4h}	−36792.623198		339.6	40	0(40)

[a] The values of E_{rel} and *N*(Cu−Cu) given in parentheses were obtained with effective core potential calculations reported in references.

tions[17] shown in brackets. Overall, the geometries of the clusters obtained by the ECP method and those reported in this work are very similar. The ECP internuclear distances are slightly less (<0.1 Å) than those obtained with our all-electron calculations. A recent experimental investigation of copper sulfide complexes, the average Cu oxidation state was close to 1, in solution using extended X-ray adsorption fine structure spectroscopy (EXAFS)[29] found that the Cu−S interatomic distances ranged between 2.3 and 2.33 Å and Cu−Cu distances between 2.72 and 2.75 Å. The average values for the interatomic distances for both Cu−S and Cu−Cu bonds obtained in our study are closer to the experimental ones than those obtained with the ECP calculations. Table 2 lists the total, relative and bonding energies of **1**−**16** along with the symmetry and the number of Cu−S and Cu−Cu bonds. The values in parentheses were obtained using ECPs as reported in ref 17.

The figures (Figure 1 includes **1**, **2**, **3**, **4**, and **5**; Figure 2 includes **6**, **7**, and **8**; Figure 3 includes **9**, **10**, and **11**; Figure 4 includes **12** and **13**; Figure 5 includes **14** and **15**; Figure 6 includes **16**) display the molecular graphs of Cu_2S and the clusters obtained with AIM2000. Bond critical points (BCPs) are shown as red spheres. Isomers are numbered in order of decreasing stability. The connectivity shown in the molecular graphs of **1**−**16** differs significantly from bonding implied in the graphical representations of the structures reported by Ahlrichs and co-workers.[15−17] Although all of the Cu−S bonds shown in the graphical structures reported by Ahlrichs and co-workers[15−17] are recovered in the AIM analysis, many of the Cu−Cu bonds are not. Even in **1**, the simplest case, there is no bond path connecting the copper atoms indicating that there is no covalent bond between them. This observation runs counter to the conclusion reached by Ahlrichs and co-workers[30] that

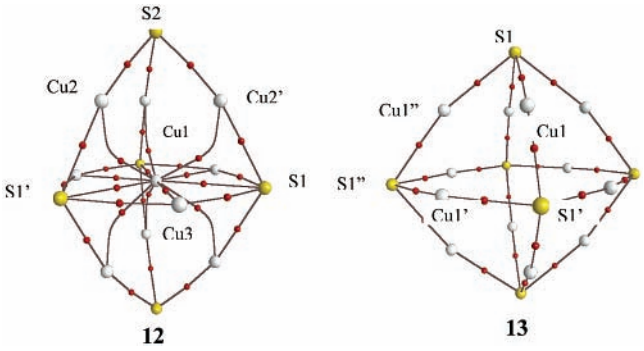

Figure 4. Displays of the molecular graphs of **12** ($Cu_{10}S_5$) and **13** $Cu_{12}S_6$; copper atoms shown as gray spheres, sulfur atoms as yellow spheres, and bond critical points as red spheres.

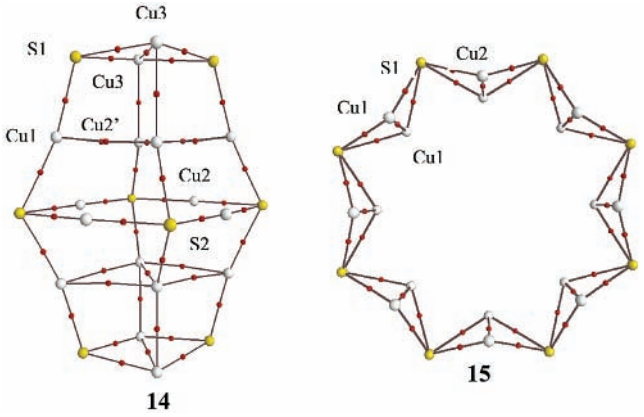

Figure 5. Display of the molecular graphs of **14** and **15** that are $Cu_{16}S_8$ isomers; copper atoms shown as gray spheres, sulfur atoms as yellow spheres, and bond critical points as red spheres.

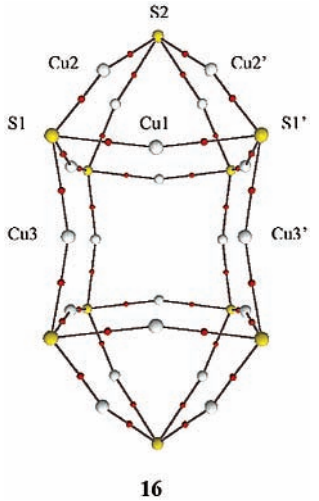

Figure 6. Display of the molecular graph of **16** ($Cu_{20}S_{10}$); copper atoms shown as gray spheres, sulfur atoms as yellow spheres, and bond critical points as red spheres.

the bonding between the coppers is covalent in character (25%) on the basis of an overlap population analysis. We find only two Cu−Cu bond paths in **2** and one in **3**. There are no bond paths between Cu1−Cu2, Cu1−Cu2′ Cu1′−Cu2, and Cu1′−Cu2′ corresponding to the connections reported previously.[17] In **4**, there are only three Cu−Cu bond paths. There is no covalent bonding between Cu2−Cu3 and Cu2′−Cu3. Only in the case of **5** does the graphical structure match the molecular graph. Cluster **6** exhibits only three Cu−Cu bond paths, showing six fewer connections than represented in ref 17. Cluster **7** also exhibits only three Cu−Cu bond paths, not the nine bonds implied in ref 17. There are no covalent bonds between Cu1−Cu1′, Cu1−Cu1″, Cu1′−Cu1″, Cu1−Cu2, Cu1−Cu2′, Cu1′−Cu2″, Cu1′−Cu2′, Cu1″−Cu2, and Cu1″−Cu2″. There are no bond paths connecting Cu2−Cu3, Cu2−Cu3′, Cu2−Cu2′, Cu2′−Cu3, and Cu2′−Cu3′ in **8**. Cluster **10** exhibits eight fewer Cu−Cu bond paths than shown in ref 17; there is no covalent bonding between Cu1−Cu2, Cu1−Cu5, Cu2−Cu4, and Cu3−Cu4 and the corresponding symmetry related atoms. Eight covalent Cu−Cu interactions that include Cu1−Cu2, Cu1′−Cu2′, and symmetry related pairs are not confirmed in cluster **11**. Of the 21 Cu−Cu connections reported in the graphical structure of cluster **12**,[17] only nine covalent bonding interactions are confirmed by bond paths, covalent Cu−Cu interactions that involve Cu2−Cu2′, Cu2−Cu3, Cu2′−Cu3, and symmetry-related pairs are not realized. No Cu−Cu covalent bonding interactions are found in clusters **13** and **16.** Thus, 24 and 40 Cu−Cu bonds are not confirmed by AIM in **13** and **16**, respectively. Although the lack of BPs between the Cu atoms could be explained on the basis of the internuclear distance that should be in range of 2.65 Å, two covalent radii, as suggested in ref 31. However**,** this appears not to be the sole factor. BPs are found between Cu2−Cu2′ of **2** where the internuclear distance is 2.73 Å, Cu2−Cu2′ of **7 (**2.74 Å), and Cu2−Cu3 (2.75 Å) of **11**. Moreover, there are no bonds between Cu atoms with shorter internuclear distances; Cu1−Cu1′ (2.63 Å) of **1**, Cu2−Cu3 (2.56 Å) of **4**, Cu1−Cu2 (2.57 Å) of **6**, Cu1 and Cu2 (2.57 Å of **7**, Cu1−Cu3 (2.63 Å) of **10**, Cu1−Cu1′ (2.56 Å) of **13**, Cu1−Cu2 (2.63 Å), and Cu2−Cu2′ (2.53 Å) of **16**. It is clear that covalent bonding assigned/assumed on the basis of internuclear distance can be in error. For example, Cu1 of **6** and **11** is simply tricoordinate not pentacoordinate.[17,31]

According to the Lewis definition, chemical bonding results from either a transfer of electrons from one atom to another (ionic bonding) or sharing electrons between atoms (covalent bonding). Contour plots of electron density ρ in selected planes of **1**, **7**, and **2** are displayed in Figure 7. Figure 7a is a display of ρ in the Cu−S−Cu plane of **1**. It is seen from Figure 7a that there are two local density minima along the geometrical lines connecting the Cu and S atoms with the BCPs shown as crosses. The extrema that exhibit minimum along the axis connecting atoms and maxima in the two other perpendicular directions are BCPs.[18] The line that follows the ridge of maximum electron density passing through BCP is the bond path (BP). In Figures 1−6, the BCPs are identified as red spheres. Existence of a BCP is the only evidence of a transfer or partitioning of electron density between atoms and consequently the presence of chemical bond between them.[18] From Figure 7a one can see that there is no local maximum in $\rho(\mathbf{r})$ in the direction perpendicular to the axis connecting the two copper atoms. The density shows only the smooth monotonic slope between Cu1−Cu1′, and there is no bond path linking them.

Figure 7b is a contour plot of $\rho(\mathbf{r})$ in the plane defined by S1, S2, and S3 of **7**. The copper atoms Cu1, Cu1′, and Cu1″ lie very nearly in this plane and the Cu_2S units are clearly seen in this plot. Although there is no saddle point in $\rho(\mathbf{r})$ and no BCP along the geometrical line between the Cu atoms, there is a ring critical point (RCP) that represents a binding element of the S1−Cu1′−S2−Cu1″−S3−Cu1 ring. The Cu−S BCPs that lie below the S1−S2−S3 plane are shown as dashed crosses. Figure 7c is a contour plot of $\rho(\mathbf{r})$ in the plane defined by S1, Cu1, S2, and Cu1′ of **2**. Even though the Cu_2S units are also recognizable in this plane, there is BCP between Cu1 and Cu1′. The density at this BCP is lower than the density at Cu−S BCPs.

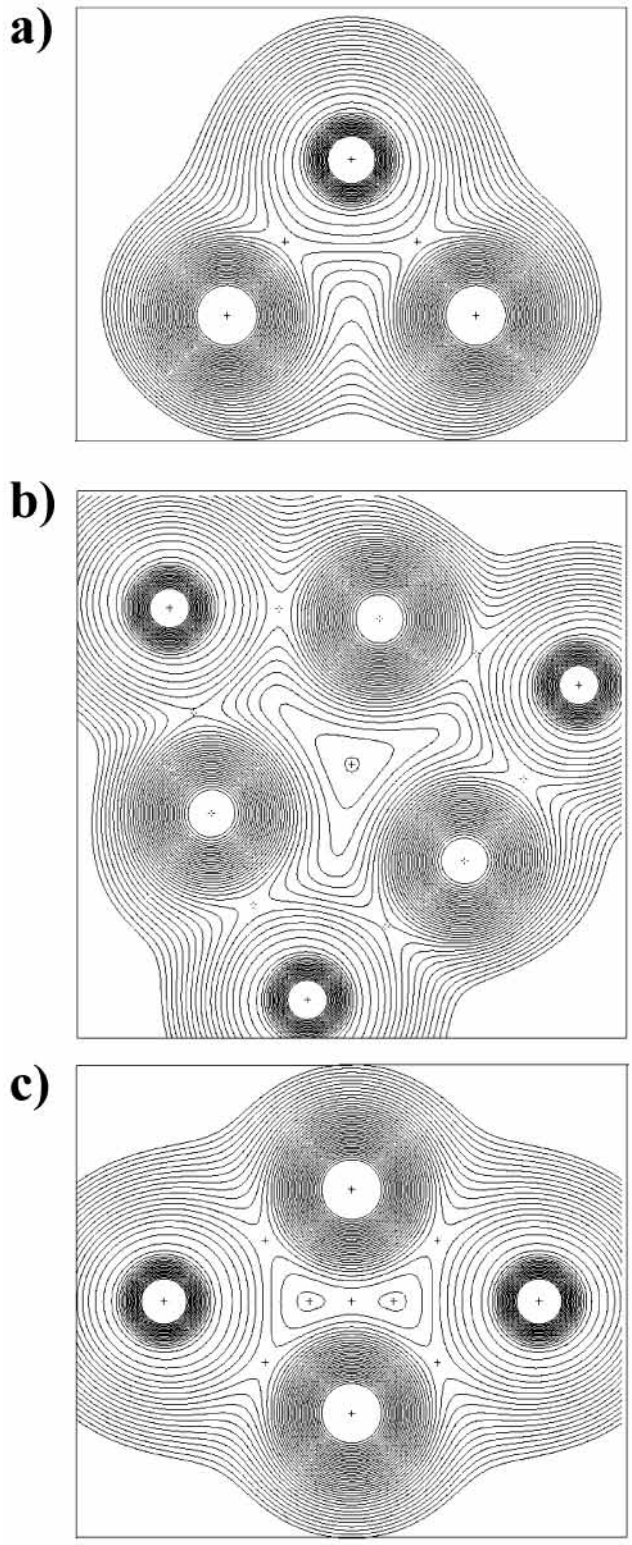

Figure 7. Contour plots of $\rho(\mathbf{r})$ in selected planes: (a) **1**, in-plane BCPs shown as crosses; (b) **7**, the S1−S2−S3 plane with the Cu−S BCPs below the S1−S2−S3 plane shown as dashed crosses; (c) **2**, the S1−Cu1−S2−Cu1′ plane with the BCPs and RCPs shown as crosses.

Even though there are no bond paths between many of the copper atoms, it is conceivable that the interactions are homoconjugative in nature. Cremer and co-workers were the first researchers to describe homoaromaticity, the interactions between atoms are of the 1,N type with N being greater than 2, on the basis of AIM theory.[32] Later Cremer and co-workers carried out a systematic investigation of a number of homoaromatic species[33] and concluded that the trishomocyclopropenyl carbocation was among the species that are stabilized by no-bond homoconjugation.[34] The method of choice for probing 1,N homoconjugation is to determine the magnitude of the delocalization indices between atoms.[35−39] However, given the size of the Cu_2S clusters involved, the evaluation of the delocalization indices must await the parallelization of PROAIMV of the AIMPAC suite of programs, a task that we plan to undertake soon.

The contour plots displayed in Figure 7 illustrate the charge distribution in typical building blocks of copper sulfide clusters. Indeed, the rhombic structure S1−Cu1−S2−Cu1′ of cluster **2**, sometimes slightly deformed can be seen in clusters **3**, **4**, **5**, **6**, **8**, **10**, **11**, and **14**. The Cu_3S_3 ring of cluster **7** comes as a composite element in construction of clusters: **9** (S1−Cu2−S2−Cu4−S2′-Cu3′), of cluster **10** (S1−Cu3−S2−Cu4−S3−Cu1), of cluster **12** (S1−Cu2−S2−Cu2′-S1′-Cu3), of cluster **13** (S1−Cu1−S1′-Cu1′-S″-Cu1″), and of cluster **16**(S1−Cu2−S2−Cu2′-S′-Cu1). Although this Cu_3S_3 is slightly deformed in bigger clusters, still the chemical structure remain the same as in **7**. It has been suggested that similar Cu_3S_3 units are likely to form on the (111) surface of Cu with common S impurities.[40] It was shown that formation and diffusion of Cu_3S_3 clusters on the Cu (111) surface is energetically more favorable.

The values of $\rho(\mathbf{r})$ and its Laplacian ($\nabla^2\rho(\mathbf{r})$) at the Cu−S and Cu−Cu BCPs are collected in Table 3. Bader[18] has used the values of $\rho(\mathbf{r}_c)$ and $\nabla^2\rho(\mathbf{r})$) at BCPs to classify bonding interactions that are produced by sharing of electrons in covalent homonuclear and heteronuclear polar bonds.[18] Large values of $\rho(\mathbf{r}_c)$ and large negative values of $\nabla^2\rho(\mathbf{r})$ are typical for shared covalent interactions. For example, the C−C covalent bond in ethane is characterized by values of $+1.70$ eA^{-3} and -15.94 eA^{-5} for $\rho(\mathbf{r}_c)$ and $\nabla^2\rho(\mathbf{r})$, respectively.[18] The polar bond O−H of H_2O exhibits values of $+2.64$ eA^{-3} and -58.84 eA^{-5}. Closed shell interactions that are found in noble gas repulsive states, ionic bonds, and hydrogen bonds are characterized by the low values of $\rho(\mathbf{r}_c)$ and a positive Laplacian. For example, the BCP of LiCl exhibits values of 0.31 eA^{-3} and 6.40 eA^{-5} for $\rho(\mathbf{r}_c)$ and $\nabla^2\rho(\mathbf{r})$, respectively. Bonds that can be viewed as being halfway between the shared and closed shell types exhibit intermediate values at the BCPs. Based on the data accumulated for molecules **1**−**16** (Table 3), the Cu−S and Cu−Cu bonds belong in the intermediate category, and the Cu−S bonds have more covalent character then Cu−Cu bonds. In both cases, $\nabla^2\rho(\mathbf{r})$ is negative, whereas $\rho(\mathbf{r}_c)$ is larger for the Cu−S than for Cu−Cu bonds.

For shared interactions, the amount of electron density partitioned by two atoms physically determines how strong the atoms are covalently bound. Therefore, the value of electron density at BCP can be taken as a measure of the strength of a bonding interaction if the same types of bonds are compared. A plot of $\rho(\mathbf{r}_c)$ versus internuclear distance (Figure 8) for the Cu−S bonds of **1**−**16** shows a clear trend; the value of $\rho(\mathbf{r}_c)$ increases as the internuclear distance decreases. A similar result was obtained in an investigation of metal−oxide complexes.[41,42] That $\rho(\mathbf{r}_c)$ is substantially smaller for the Cu−Cu BCPs than the Cu−S BCPs suggests that the covalent bonding between Cu−Cu bonds is weaker than between the Cu−S bonds (Figure 9). A comparison of $\rho(\mathbf{r}_c)$ values of a number of Cu−S bonds indicates that the bond strength depends on the coordination number. In the case of **4**, the Cu2−S1 bond to three-coordinate S1 exhibits a significantly larger $\rho(\mathbf{r}_c)$ value (0.51 eA^{-3}) than the Cu2−S2 bond to four-coordinate S2 (0.38). In **11**, the Cu1−S1 bond between four-coordinate S and three-coordinate Cu may

TABLE 3: Values of the Density (e Å^{-3}) and the Laplacian (e Å^{-5}) at bond Critical Points

compound	S1−Cu1	S1−Cu2	S1−Cu3	S2−Cu2	Cu1−Cu1′	Cu1−Cu2	Cu1−Cu3	Cu2−Cu3	Cu2−Cu2′	Cu3−Cu3′
1	0.67									
	−1.164[a]									
2	0.48	0.64			0.34				0.18	
	−0.89	*−1.103*			*−0.56*				*−0.29*	
3	0.50	0.65			0.34					
	−0.89	*−1.13*			*−0.58*					
4	0.52	0.51		0.38		0.31			0.30	
	−0.95	*−0.94*		*−0.65*		*−0.50*			*−0.50*	
5	0.40				0.34					
	−0.69				*−0.56*					
6	0.45				0.34					
	−0.79				*−0.58*					
7	0.46	0.55							0.14	
	−0.95	*−0.95*							*−0.33*	
8	0.38	0.49		0.55		0.23	0.18			0.27
	−0.82	*−0.77*		*−1.08*		*−0.48*	*−0.37*			*−0.67*
9	0.48	0.52	0.42	0.57				0.33		
	−0.86	*−0.94*	*−0.70*	*−1.04*				*−0.51*		
10	0.52	0.39	0.38	0.53				0.33	0.25	
	−0.96	*−0.67*	*−0.73*	*−0.97*				*−0.53*	*−0.34*	
11	0.49	0.43			0.33			0.17		
	−0.94	*−0.75*			*−0.55*			*−0.31*		
12	0.32	0.68	0.53	0.46		0.31	0.48			
	−0.67	*−1.15*	*−0.66*	*−1.10*		*−0.47*	*-0.89*			
13	0.47									
	−0.82									
14	0.62		0.51	0.45		0.17		0.29	0.21	0.32
	−1.23		*−0.98*	*−0.80*		*−0.29*		*−0.41*	*−0.36*	*−0.54*
15	0.50				0.29					
	−0.94				*−0.51*					
16	0.53	0.52	0.55	0.51						
	−0.99	*−1.03*	*−1.11*	*−0.94*						

[a] Values of the Laplacian are given in italics.

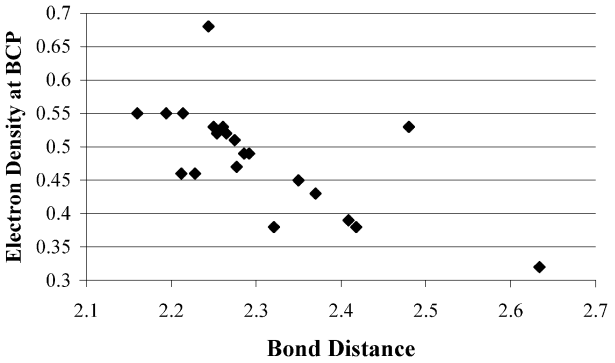

Figure 8. Plot of $\rho(\mathbf{r})$ at the bond critical point versus Cu−S internuclear distance.

be stronger (0.49) than the Cu2−S1 bond connecting four-coordinate S to a four-coordinate Cu (0.43). Additional support for this view is provided by a comparison of the Cu1−S1 bonds of **3** where three-coordinate Cu is bonded to three-coordinate S and **6** where three-coordinate Cu is bonded to four-coordinate S.

Conclusions about bond strength made on the basis of interatomic distance could be misleading. Indeed, according to suggestions by refs 15−17, the Cu−S bond between six coordinate Cu and four coordinate S of cluster **13** should be weaker than that between four coordinate Cu and four coordinate S of cluster **5**. The values of $\rho(\mathbf{r}_c)$ given by AIM in Table 3, however, show that the reverse situation might be the case with the ρ values being 0.47 and 0.40, respectively. Another example of possible misinterpretation of bond strength and coordination is seen in cluster **10**. According to Ahlrichs and co-workers,[17] the bond Cu1−S1 of nine-coordinate Cu1 with five-coordinate S1 should be weaker than the bond Cu2−S1 of seven-coordinate Cu2 with the same sulfur. However, ρ values of 0.52 and 0.39 seen in the AIM analysis for these bonds suggests that the opposite may be the case here as well. The dependence of the ρ value on the degree of coordination implies that the strength of the bond with the same local environment should be transferable from one molecule to another. Indeed, one may notice nearly equivalent values of ρ for similar bonds in different clusters; S1−Cu1 in clusters **2** and **3**, S1−Cu1 in clusters **6** and **11**, S1−Cu1 of **13** and S2−Cu2 of **16**, and Cu1−Cu1′ of **2**, **3**, **6**, **11** (Table 3). A quantitative evaluation of bond strength by via $\rho(\mathbf{r}_c)$ is very important not only because of transferability between molecules but also because an estimate of bond strength may be difficult to obtain in some cases. For example in cyclic molecules such as **5**−**16**, it is almost impossible to break one bond leaving intact the others. Therefore, the evaluation of dissociation energy for such bonds would be approximate due to averaging. Atomic coordination and individual bond strengths are very important factors that determine the stability and reactivity of molecular structures. According to Ahlrichs and co-workers,[15−17] the number of Cu−Cu bonds was comparable and sometimes exceeded the number of Cu−S bonds thus substantially contributing to cluster stability (Table 2). However, because fewer Cu−Cu bonds were revealed than previously suggested and because Cu−S bonds are stronger than Cu−Cu bonds, one should conclude that the stability of copper sulfides is mostly determined by the Cu−S interactions. EXAFS investigations of copper sulfides in solution[29] support predominant connectivity of Cu atoms with S rather than with Cu. For example, it was found that every Cu was surrounded by three or four sulfur atoms but by only one copper atom.

We wish to propose an explanation for the asymptotic behavior of stabilization energy versus number of Cu_2S units where a maximum is reached at a cluster size with $n > 6$. The

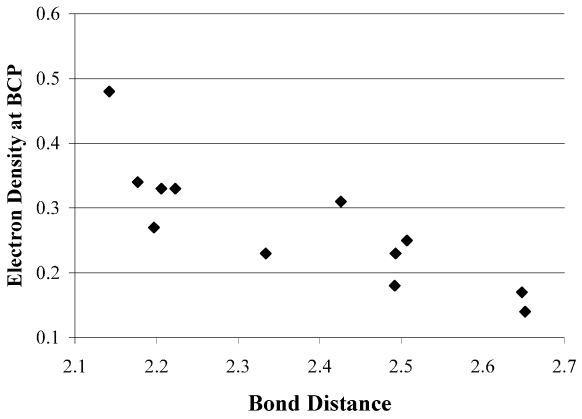

Figure 9. Plot of $\rho(\mathbf{r})$ at the bond critical point versus Cu−Cu internuclear distance.

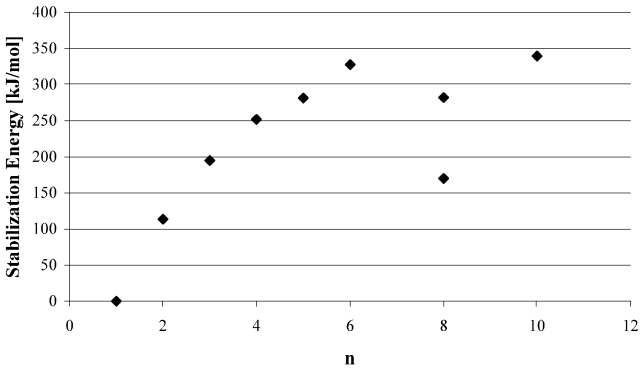

Figure 10. Graph of the stabilization energy (E_n) versus the number of Cu_2S units (n).

stabilization energies per monomer unit E_n given by eq 1[17, 31] are

$$E_n = 1/n\, E(Cu_2S)_n - E(Cu_2S) \qquad (1)$$

collected in Table 2. First, we attempted to find stable clusters of composition $Cu_{16}S_8$ between $Cu_{12}S_6$ and $Cu_{20}S_{10}$ to confirm the saturation of stabilization energy with increasing size and located **14** and **15** that are shown in Figure 4. Cluster **15** can be viewed as a logical extrapolation/expansion of **6** and **11**. Cluster **14** is a combination of **2** and **13**. The plot of stabilization energy versus the number of Cu_2S units is given in Figure 10. As seen from the data in Table 2 and the plot, the stabilization energy per Cu_2S unit of both clusters deviates significantly from the values seen for **13** and **16** and correlate with values that are typical for the smaller clusters such as Cu_6S_3 and $Cu_{10}S_5$, respectively. This low E_n suggests a reason $Cu_{16}S_8$ clusters have not been found experimentally. E_n can be physically interpreted as the potential energy of interaction of one unit with the others. The greater number of Cu_2S units that are bonded with each other, the higher stabilization energy per unit is obtained. For example in **2**, the Cu1−S−Cu2 unit interacts with the Cu2′−S2−Cu1′ unit via the Cu1−S2, Cu1−Cu1′, and Cu2−Cu2′ bonds. In **10**, Cu1−S1−Cu2 is bonded with three other units, Cu3−S2−Cu4, Cu5−S3−Cu4′, and Cu2′−S2′−Cu3′. If we define the term unit coordination that is the number of Cu_2S units bonded to a given one, and every Cu_2S unit is always represented by one sulfur atom, it is possible to determine the number of bonded units simply by number of S atoms directly connected through coppers to the sulfur of a given unit. In this sense, every Cu_2S fragment of isomers **2**−**5** is bonded to only one other unit. Those in isomers **6**−**8** are two-unit coordinated. Every Cu_2S unit of **9** is three-unit coordinated. Two Cu_2S units of **10** are two-unit coordinated (bridged with S2 and S2′), and two others are three-unit coordinated (bridged with S1 and S3). The stabilization energy per unit is higher for clusters with higher unit-coordination. Thus, one can see why four-unit coordinated clusters **13** and **16** have higher stabilization energies than the two unit-coordinated cluster **15**. It is seen that clusters with the same unit coordination exhibit similar E_n's. For example, two-unit coordinated clusters **6**, **11**, and **15** do not substantially differ in stabilization energy while being substantially different in size. Clusters **13** and **16** have maximum four-unit coordination among all investigated structures and, consequently, the highest stabilization energies. Higher unit coordination can be found in bulk crystalline Cu_2S nanowires[9,10] or in the mineral chalcocite[43] because of twinning. However, it is difficult to imagine the small Cu_2S clusters with coordination higher than four.

Conclusions

All-electron calculations at the Becke3PW91/6-311+G(d) level yield geometries of $(Cu_2S)_n$ clusters that compare favorably with those obtained by other researchers at the MP2(ECP) level. In fact, on average, the Becke3PW91/6-311+G(d) internuclear distances are closer to experimental values obtained with EXAFS than those obtained at the MP2(ECP). Covalent bonding of Cu−Cu atoms is not simply determined by interatomic distance. Three new clusters, one of composition Cu_8S_4 and two of composition $Cu_{16}S_8$ have been studied. Covalent bonding between copper atoms previously assigned on the basis of internuclear distance and overlap populations is not realized in AIM analyses. As a result, the stability of copper(I) sulfides depends predominately on the number of covalent Cu−S bonds that are present in the cluster rather than on Cu−Cu shared interactions. The asymptotic behavior of the stabilization energy with increasing cluster size can be explained on the basis of unit coordination. It is predicted that four-unit coordination is the source of the limiting maximum stabilization seen in the case of $(Cu_2S)_n$ clusters with $n > 7$.

Acknowledgment. We thank SHARCNET (Shared Hierarchical Academic Research Computing Network (of Ontario) for providing computing resources at McMaster University. We gratefully acknowledge financial support by the Natural Sciences and Engineering Research Council of Canada.

References and Notes

(1) Beinert, H.; Holm, R. H.; Munck, E. *Science* **1997**, *277* 653.
(2) Langen, R.; Jensen, G. M.; Jacob, U.; Stephens, P. J.; Warshel, A. *J. Biol. Chem.* **1992**, *267*, 25625.
(3) Zhou, J.; Raebiger, J. W.; Crawford, C. A.; Holm, R. H. *J. Am. Chem. Soc.* **1997**, *119*, 6242.
(4) Bae, W.; Mehra, R. K. *J. Inorg. Biochem.* **1998**, *70*, 125.
(5) Rasmussen, T.; Berks, B. C.; Sanders-Loehr, J.; Dooley, D. M.; Zumft, W. G.; Thomson, A. J. *Biochemistry* **2000**, *39*, 12753.
(6) Chou, H. C.; Rohatgi, A.; Jokerst, N. M.; Kamra, S.; Stock, S. R.; Lowrie, S. L.; Ahrenkiel, R. K.; Levi, D. H. *Mater. Chem. Phys.* **1996**, *43*, 178.
(7) Niemegeers, A.; Burgelman, M. *J. Appl. Phys.* **1997**, *81*, 2881.
(8) Shi, S.; Xin, X. Q. *Mater. Res. Soc. Symp. Proc.* **1995**, *374*, 151.
(9) Wang, S.; Yang, S.; Dai, Z. R.; Wang, Z. L. *Chem. Mater.* **2001**, *13*, 4794.
(10) Wang, S.; Yang, S. *Phys. Chem. Chem. Phys.* **2001**, *3*, 3750.
(11) Bowles, K. C.; Bell, R. A.; Ernste, M. J.; Kramer, J. R.; Manolopoulos, H.; Ogden, N. *Environ Toxicolog. Chem.* **2002**, *21*, 693.
(12) Bowles, K. C.; Bianchini, A.; Brauner, C. J.; Kramer, J. R.; Wood, C M. *Environ. Toxicolog. Chem.* **2001**, *21*, 1283. Bianchini, A.; Bowles, K. C.; Brauner, C. J.; Gorsuch, J. W.; Kramer, J. R.; Wood, C. M. *Environ. Toxicol. Chem.* **2001**, *21*, 1290.

(13) Mouesca, J. M.; Chen, J. L.; Noodleman, L.; Bashford, D.; Case, D. A. *J. Am. Chem. Soc.* **1994**, *116*, 11898−11914.
(14) Noodleman, L.; Case, D. A. *Adv. Inorg. Chem.* **1992**, *38*, 423.
(15) Dehnen, S.; Eichhofer, A.; Fenske, D. *Eur. J. Inorg. Chem.* **2002**, 279−317.
(16) Eichorn, K.; Dehnen, S.; Ahlrichs, R. *Chem. Phys. Lett.* **1998**, *284*, 287.
(17) Dehnen, S.; Schafer A.; Ahlrichs, R.; Fenske, D. *Chem. Eur. J.* **1996**, 429.
(18) Bader, R. F. W. *Atoms in Molecules*; Oxford Science Publications: Oxford, U.K., 1990.
(19) Perdew, J. P.; Wang, Y. *Phys. Rev. B* **1992**, *45*, 13244.
(20) Frisch, M. J.; Trucks, G. W.; Schlegel, H. B.; Scuseria, G. E.; Robb, M. A.; Cheeseman, J. R.; Zakrzewski, V. G.; Montgomery, J. A., Jr.; Stratmann, R. E.; Burant, J. C.; Dapprich, S.; Millam, J. M.; Daniels, A. D.; Kudin, K. N.; Strain, M. C.; Farkas, O.; Tomasi, J.; Barone, V.; Cossi, M.; Cammi, R.; Mennucci, B.; Pomelli, C.; Adamo, C.; Clifford, S.; Ochterski, J.; Petersson, G. A.; Ayala, P. Y.; Cui, Q.; Morokuma, K.; Malick, D. K.; Rabuck, A. D.; Raghavachari, K.; Foresman, J. B.; Cioslowski, J.; Ortiz, J. V.; Stefanov, B. B.; Liu, G.; Liashenko, A.; Piskorz, P.; Komaromi, I.; Gomperts, R.; Martin, R. L.; Fox, D. J.; Keith, T.; Al-Laham, M. A.; Peng, C. Y.; Nanayakkara, A.; Gonzalez, C.; Challacombe, M.; Gill, P. M. W.; Johnson, B. G.; Chen, W.; Wong, M. W.; Andres, J. L.; Head-Gordon, M.; Replogle, E. S.; Pople, J. A. *Gaussian 98*, revision A.9; Gaussian, Inc.: Pittsburgh, PA, 1998.
(21) Siegbahn, P. E. M. *Adv. Chem. Phys*. **1996**, *93*, 365.
(22) Wilson, S. *Adv. Chem. Phys*. **1987**, *67*, 474.
(23) Bauschlicher, C. W.; Partridge, H.; Sheehy, J. A.; Langhoff, S. R.; Rosi, M. *J. Phys. Chem.* **1992**, *96*, 6969.
(24) *HyperChem*; Hypercube, Inc., 1996.
(25) Biegler-Konig, F. W.; Bader, R. F. W.; Tang, T.-H. *J. Comput. Chem.* **1982**, *3*, 317.
(26) Biegler-Konig, F. *AIM 2000*; University of Applied Science: Bielefeld, Germany, 1998−2000.
(27) Fisher, K.; Dance, I.; Willet, G.; Yi, M. N. *J. Chem. Soc., Dalton Trans.* **1996**, 709.
(28) Fisher, K.; Dance, I. *J. Chem. Soc., Dalton Trans.* **1997**, 2831.
(29) Helz, G. R.; Charnock, J. M.; Vaughan, D. J.; Garner, C. D. *Geochim. Cosmochim. Acta* **1993**, *57*, 15.
(30) Ehrhardt, C.; Ahlrichs, R. *Theor. Chim. Acta* **1985**, *68*, 231.
(31) Schafer, A.; Ahlrichs, R. *J. Am. Chem. Soc.* **1994**, *116*, 10686.
(32) Cremer, D.; Kraka, E.; Slee, T. S.; Bader, R. F. W.; Lau, C. D. H.; Nguyen-Dang, T. T.; MacDougall, P. J. *J. Am. Chem. Soc.* **1983**, *105*, 5069.
(33) Cremer, D.; Childs, R. L.; Kraka, E. In *The Chemistry of the cyclopropyl group*; Rappoport, Z., Ed.; John Wiley & Sons Ltd: New York, 1995; Vol. 2, pp 339−410.
(34) Szabo, K. J.; Kraka, E.; Cremer, D. J. *Org. Chem.* **1996**, *61*, 2783.
(35) Bader, R. F. W.; Stephens, M. E. *J. Am. Chem. Soc.* **1975**, *97*, 7391.
(36) Fradera, X.; Austen, M. A.; Bader, R. F. W. *J. Phys. Chem. A* **1999**, *103*, 304.
(37) Molina, J. M.; Dobado, J. A.; Heard, G. L.; Bader, R. F. W.; Sundberg, M. R. *Theor. Chem. Acc.* **2001**, *105*, 365.
(38) Bader, R. F. W.; Matta, C. F. *Inorg. Chem.* **2001**, *40*, 5603.
(39) Wang Y.-G.; Werstiuk, N. H. *J. Comput. Chem.* **2002**, *23*, in press.
(40) Feibelman, P. J. *Phys. Rev. Lett.* **2000**, *85*, 606.
(41) Hill, F. C.; Gibbs, G. V.; Boisen, M. B. *Phys. Chem. Miner.* **1997**, *24*, 582
(42) Gibbs, G. V.; Boisen, M. B.; Beverly, L. L.; Rosso, K. M. *Rev. Mineral. Geochem.* **2002**, *42*, 345.
(43) Evans, H. T. Jun. *Nature Phys. Sci.* **1971**, *232*, 89.